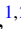




Bayesian analysis of muon capture on the deuteron in chiral effective field theoryA. Gnech ^{1,2}, L. E. Marcucci ^{3,4} and M. Viviani ⁴¹*European Center for Theoretical Studies in Nuclear Physics and Related Areas (ECT^{*}) and Fondazione Bruno Kessler, I-38123 Villazzano (TN), Italy*²*INFN-TIFPA Trento Institute of Fundamental Physics and Applications, I-38123 Trento, Italy*³*Dipartimento di Fisica E. Fermi, Università di Pisa, Pisa I-56127, Italy*⁴*Istituto Nazionale di Fisica Nucleare, Sezione di Pisa, Pisa I-56127, Italy*

(Received 15 May 2023; revised 12 February 2024; accepted 8 March 2024; published 20 March 2024)

We compute the muon capture on deuteron in the doublet hyperfine state for a variety of nuclear interactions and consistent nuclear currents. Our analysis includes a detailed examination of the theoretical uncertainties coming from different sources: the single-nucleon axial form factor, the truncation of the interaction and current chiral expansion, and the model dependence. Moreover, we study the impact of the use of different power counting scheme for the electroweak currents on the truncation error. To estimate the truncation error of the chiral expansion of interactions and currents we use the most modern techniques based on Bayesian analysis. This method enables us to give a clear statistical interpretation of the computed theoretical uncertainties. Finally, we provide the differential capture rate as function of the kinetic energy of the outgoing neutron which may be measured in future experiments. Our recommended theoretical value for the total doublet capture rate is $\Gamma_{\text{th}} = 395 \pm 10 \text{ s}^{-1}$ (68% confidence level). We calculated also the capture rate in the quartet hyperfine state, which turns out to be in the range $[13.3\text{--}13.8] \text{ s}^{-1}$ depending on the adopted nuclear interaction.

DOI: [10.1103/PhysRevC.109.035502](https://doi.org/10.1103/PhysRevC.109.035502)**I. INTRODUCTION**

The muon capture on deuteron, i.e., the process

$$\mu^- + d \rightarrow n + n + \nu_\mu \quad (1.1)$$

is one of the electroweak processes that is accessible experimentally and at the same time can be computed using the most modern theoretical nuclear physics techniques combining chiral effective field theory (χ EFT) with *ab initio* numerical methods. This makes the reaction in Eq. (1.1) the ideal system for testing χ EFT interactions and electroweak currents.

The experimental results for the total capture rate in the initial doublet hyperfine state Γ [1–4] are relatively old and have large error bars that make them compatible within each other but hard to use for precision tests of the theory. To improve the precision of experimental measurements, an ongoing experiment at the Paul Scherrer Institute, in Switzerland, performed by the MuSun Collaboration, aims to reduce the uncertainty at the order of $\approx 1.5\%$ [5]. If such precision is achieved, then it will enable more stringent test of the χ EFT predictions.

On the theory side, several calculations have been carried out. A review of the theoretical results from up to the early 2010s can be found in Ref. [6]. Some more recent calculations, but not yet fully within the χ EFT framework, have been performed also in Refs. [7,8]. The first steps within the “hybrid” χ EFT approach, where phenomenological potentials are used together with χ EFT nuclear currents, have been performed in Refs. [7,9]. On the other hand, the first fully consistent χ EFT calculations are those of Refs. [10,11]. Note that the results of Ref. [10], as well as those of Ref. [11], were affected by a widely spread error in the relation between the

low-energy constant (LEC) entering the three-nucleon interaction and that one entering the axial current. In Ref. [12] such error was spotted and the results of Ref. [10] were corrected. Over the past few years, a fully consistent χ EFT calculation, not affected by the above-mentioned error, has been performed [13]. This work addressed also the impact of the experimental uncertainty on the single-nucleon axial form factor [14]. The work in Ref. [13] retained only the 1S_0 channel while in that of Bonilla *et al.* [15] a complete partial wave expansion was performed together with an analysis of the theoretical uncertainties to study the capture rate in both the $f = 1/2$ (doublet) and $f = 3/2$ (quartet) hyperfine states.

This work moves on a parallel line, starting from our recent paper where we considered only the 1S_0 neutron-neutron channel [16]. We complete the calculation of Ref. [16] adding the missing channels with a dual purpose. The first is to have the most robust theoretical error estimate based on the Bayesian analysis of the truncation errors of the chiral current and interaction expansions, on the model dependence, and on the propagation of the uncertainties related to the LECs appearing in the currents. Moreover, we carry on also an analysis of the impact of the use of different power counting for the electroweak currents on the truncation errors. For the Bayesian analysis we use the approach introduced in Ref. [17] and already employed in several works to give reliable estimates of truncation errors in chiral effective field theory (see Ref. [18] for a complete list of works). The second purpose is to compute the spectra of the outgoing neutrons as function of the kinetic energy of the neutron. Beyond the technical details, this kind of spectrum can possibly be measured in MuSun experiment [19] and can be useful for the simulation

of the experimental apparatus, and consequently for data analysis.

The paper is organized as follow. In the next section we will introduce the theoretical formalism giving the explicit expression for the differential capture rate as function of the kinetic energy of the neutron. In Sec. III we present the nuclear interaction and current models used in this work. Section IV is dedicated to a detailed examination of the theoretical uncertainties. In Sec. V, we discuss our results comparing them with the recent literature. Finally, in Sec. VI we consider the impact of our results on the analysis of the future data of the MuSun experiment.

II. MUON CAPTURE ON DEUTERON FUNDAMENTALS

In the literature the muon capture differential capture rate was computed versus the relative momenta of the two emitted neutrons. This has the advantage to reduce the numerical effort needed in the calculation. On the other hand, this is not what can be measured experimentally. In this work we consider the differential capture rate as function of the kinetic energy of one of the emitted neutrons (i.e., $E'_1 = E_1 - m_n$), which is the quantity that can potentially be measured in an experiment using a neutron detector. Let us begin with the Fermi golden rule, that reads

$$d\Gamma = (2\pi)\delta(E_1 + E_2 + k_\nu - m_\mu - m_d) \overline{|T_{fi}|^2} \frac{d\mathbf{p}_1}{(2\pi)^3} \frac{d\mathbf{k}_\nu}{(2\pi)^3}, \quad (2.1)$$

where $E_1(E_2)$ is the energy of the first (second) outgoing neutron, k_ν the energy of the emitted neutrino, $\mathbf{p}_1(\mathbf{p}_2)$ the momenta of the first (second) outgoing neutron, and \mathbf{k}_ν the momentum of the outgoing neutrino. Note that the phase space of the second emitted neutron has been eliminated using the conservation of the momenta. The transition amplitude is written as in Ref. [7],

$$\overline{|T_{fi}|^2} = \frac{1}{2f+1} \sum_{s_1, s_2, h_\nu} \sum_{f_z} |T_{fi}(f, f_z; s_1, s_2, h_\nu)|^2, \quad (2.2)$$

where f, f_z indicate the initial hyperfine state, while s_1, s_2 , and h_ν denote the spin z projection for the two neutrons and the neutrino helicity state. In turn, $T_{fi}(f, f_z; s_1, s_2, h_\nu)$ is given by

$$\begin{aligned} T_{fi}(f, f_z; s_1, s_2, h_\nu) &\equiv \langle nn, s_1, s_2; \nu, h_\nu | H_W | (\mu, d); f, f_z \rangle \\ &\simeq \frac{G'_V}{\sqrt{2}} \psi_{1s} M_{fi}(f, f_z; s_1, s_2, h_\nu), \end{aligned} \quad (2.3)$$

where we have defined

$$\begin{aligned} M_{fi}(f, f_z; s_1, s_2, h_\nu) &= \sum_{s_\mu, s_d} \left\langle \frac{1}{2} s_\mu, 1 s_d \left| f f_z \right. \right\rangle l_\sigma(h_\nu, s_\mu) \\ &\times \langle \Psi_{\mathbf{p}, s_1 s_2}(nn) | j^\sigma(\mathbf{q}) | \Psi_{s_d}(d) \rangle, \end{aligned} \quad (2.4)$$

with l_σ and j^σ being the leptonic and hadronic current densities, respectively [7]. Here the leptonic momentum transfer \mathbf{q} is defined as $\mathbf{q} \simeq -\mathbf{k}_\nu$ and $\mathbf{p} = (\mathbf{p}_1 - \mathbf{p}_2)/2$ is the relative momentum among the two neutrons. Furthermore, $\Psi_d(s_d)$ and $\Psi_{\mathbf{p}, s_1 s_2}(nn)$ are the deuteron and final nn wave functions, respectively, with s_d indicating the deuteron

spin z projection, which is computed using the variational method described in Refs. [7,16]. The final nn wave function $\Psi_{\mathbf{p}, s_1 s_2}(nn)$ can be expanded in partial waves as

$$\begin{aligned} \Psi_{\mathbf{p}, s_1 s_2}(nn) &= 4\pi \sum_S \left\langle \frac{1}{2} s_1, \frac{1}{2} s_2 \left| SS_z \right. \right\rangle \sum_{LL_z JJ_z} i^L Y_{LL_z}^*(\hat{\mathbf{p}}) \\ &\times \langle SS_z, LL_z | JJ_z \rangle \overline{\Psi}_{nn}^{LSJJ_z}(p), \end{aligned} \quad (2.5)$$

where $\overline{\Psi}_{nn}^{LSJJ_z}(p)$ is the nn wave function with orbital angular momentum LL_z , total spin SS_z , and total angular momentum JJ_z that is computed numerically by using the Kohn variational principle (see Ref. [20]). The calculation is performed using partial waves up to $J = 4$. The contribution to the total capture rate of the partial waves with $J > 2$ is of the order of 0.75%. We verified that partial waves with $J > 4$ give negligible contributions. Finally, in Eq. (2.3), the function ψ_{1s} is the average over the nuclear volume of the muon wave function in $1s$ orbit [7,21], namely

$$|\psi_{1s}| \simeq |\psi_{1s}^{\text{av}}| \equiv |\psi_{1s}(0)| = \sqrt{\frac{(\alpha \mu_{\mu d})^3}{\pi}}, \quad (2.6)$$

where $\psi_{1s}(0)$ denotes the Bohr wave function for a point charge e evaluated at the origin, $\mu_{\mu d}$ is the reduced mass of the (μ, d) system, and α is the fine-structure constant. The integration of the matrix elements M_{fi} is performed using Gaussian-Legendre quadrature with ≈ 45 points on the angles and ≈ 80 on the internucleon distance r . This permits full convergence of the integrals.

Without losing generality we can choose $\mathbf{q} \parallel \hat{z}$ and define the angle θ_1 as the angle between \mathbf{q} and \mathbf{p}_1 . After exploiting the conservation of energy in Eq. (2.1) the differential capture rate reads

$$\begin{aligned} \Gamma^f(E'_1) &= \frac{G_V'^2}{\pi} |\psi_{1s}(0)|^2 E_1 p_1 \int d \cos \theta_1 \frac{E_2 k_\nu^2}{E_2 + k_\nu + p_1 \cos \theta_1} \\ &\times \sum_{s_1 s_2 h_\nu} \sum_{f_z} |M_{fi}(f, f_z, s_1, s_2, h_\nu; p_1, \cos \theta_1)|^2, \end{aligned} \quad (2.7)$$

where k_ν and E_2 can be easily obtained by the momentum and energy conservation. The superscript f , that can be equal to 1/2 and 3/2, indicates the hyperfine state for which the capture rate is computed. Note that in this case the scattering wave function depends explicitly on p_1 and $\cos \theta_1$ through \mathbf{p} making the calculation much more expensive.

The total capture rate is then computed integrating directly on the kinetic energy E_1

$$\Gamma^f = \int_0^{E_1^{\text{max}}} dE'_1 \Gamma^f(E'_1). \quad (2.8)$$

The integrations on E'_1 and $\cos \theta_1$ has been performed using Gauss-Legendre quadrature. To reach convergence we need to use at least 50 points on E'_1 and 20 on $\cos \theta_1$. The total capture rate was also computed using the standard approach as in Ref. [7], obtaining on the total capture rate numerical differences below 0.1 s^{-1} for each nuclear interaction considered. In Table I we report the constants and the masses used in this work. Note that the vector coupling constant that first

TABLE I. Values of the constants used in the present calculation.

G'_V	$1.149 \times 10^{-11} \text{ MeV}^{-2}$
$1/\alpha$	137.04
m_d	1875.61 MeV
m_n	939.57 MeV
m_μ	105.66 MeV

appears in Eq. (2.3) is

$$G_V^2 = G_V^2 (1 + \Delta_R^V), \quad (2.9)$$

where the vector coupling constant G_V is given by $G_V = 1.1357 \times 10^{-11} \text{ MeV}^{-2}$, and the process independent radiative correction Δ_R^V is $\Delta_R^V = 0.02454$, according to the new updated values of Ref. [22]. The final value is then $G_V^2 = 1.149 \times 10^{-11} \text{ MeV}^{-2}$.

III. NUCLEAR INTERACTIONS AND ELECTROWEAK CURRENTS

The interactions we use in the present calculation are of two types. The first ones, developed in Norfolk (NV) [23,24], are local interactions up to the next-to-next-to-next-to-leading order (N3LO) and include Δ -isobars together with pions and nucleons as degrees of freedom. The interactions are regularized in configuration space with two regulators, one (R_S) for the short-range components associated with $2N$ contact terms and the other (R_L) for the long-range terms. We consider four different interactions of this family for which two different sets of regulators have been used. The LECs have been fitted considering the $2N$ database within two different energy ranges.

The second family of interactions considered in this work is the one developed by Entem, Machleidt and Nosyk (EMN) [25]. These interactions are implemented in momentum space and are strongly nonlocal. The degrees of freedom are pions and nucleons only. For this interaction family all the orders up to the N3LO are available for three different cutoff values $\Lambda = 450, 500, \text{ and } 550 \text{ MeV}$. The LECs of these interactions are fixed fitting the $2N$ database up to 300 MeV. In

TABLE II. Summary of $2N$ interactions used in this study. In the first column we indicate the name adopted to identify each interaction and in the remaining columns we list its main features, including degrees of freedom (DOF), chiral order (O_χ), cutoff values, laboratory-energy range over which the fits to the $2N$ database have been carried out (E range), and whether it is expressed in configuration (r) or in momentum (p) space.

Name	DOF	O_χ	(R_S, R_L) or Λ	E range	Space
NVIa	π, N, Δ	N3LO	(0.8,1.2) fm	0–125 MeV	r
NVIb	π, N, Δ	N3LO	(0.7,1.0) fm	0–125 MeV	r
NVIIa	π, N, Δ	N3LO	(0.8,1.2) fm	0–200 MeV	r
NVIIb	π, N, Δ	N3LO	(0.7,1.0) fm	0–200 MeV	r
EMN450	π, N	N3LO	450 MeV	0–300 MeV	p
EMN500	π, N	N3LO	500 MeV	0–300 MeV	p
EMN550	π, N	N3LO	550 MeV	0–300 MeV	p

TABLE III. Ordering of the chiral electroweak currents as given in Ref. [30]. Abbreviations: 1b, one-body; OPE, one-pion exchange; CT, contact terms; NR, nonrelativistic; RC, relativistic corrections; and OPE- Δ , one-pion-exchange currents with an intermediate Δ -isobar excitation. The terms in the square bracket are RC that we kept at the order given by the naive power-counting. With the star we indicate the terms that do not appear for the EMN interactions.

Oper.	LO (Q^{-3})	NLO (Q^{-2})	N2LO (Q^{-1})	N3LO (Q^0)
$\rho(A)$	—	—	1b(NR) OPE	—
$\mathbf{j}(A)$	1b(NR)	—	OPE- Δ^* [1b(RC)]	CT(d_R) OPE
$\rho(V)$	1b(NR)	—	[1b(RC)]	[OPE(RC)]
$\mathbf{j}(V)$	—	—	1b(NR) OPE	OPE- Δ^* [1b(RC)]

Table II we summarize the names of the interactions used in this work and their specific characteristics.

The adopted models for the nuclear axial and vector currents are the ones derived in Refs. [26,27] for the NV potentials and Refs. [28,29] for the EMN ones, respectively. In this work we performed the analysis on the truncation errors of the currents considering both the Bochum (see, for example, Ref. [30]) and the JLab-Pisa group power counting (see, for example, Refs. [28,29]). We summarize the various contributions to the currents for the Bochum and JLab-Pisa power counting in Tables III and IV, respectively. Note that for the Bochum power counting we considered the relativistic corrections of the same order as in the naive-power counting.¹

One of the goal of this work is to study the role of the axial contact term (CT) at N3LO and therefore of the value of the LEC d_R [see Eq. (A1)] on the determination of the total capture rate. Since the LEC d_R is linearly dependent on the LEC c_D that appears in the three-nucleon interaction, this has been determined fitting contemporary the ^3H binding energy and the Gamow-Teller matrix element of the $^3\text{H}\beta$ decay.

For the NV interactions we used the value of c_D (and c_E) fitted in Ref. [27]. For the EMN interactions we refitted c_D (and c_E) following the procedure of Ref. [27]. The results are reported in Appendix.

The calculation of the differential and total muon capture rate on deuteron presented below has been carried out for all the nuclear interactions presented in Table II and for all the chiral order from LO to N3LO in the case of the EMN interactions.

¹This has been done to maintain consistency with the LECs fitted in previous works. Clearly, this generates some theoretical inconsistency. However, from the numerical point of view the total contribution of the relativistic corrections are of the order of $\approx 1\%$ on the total capture rate, and the impact is minimal on the error analysis. For completeness we report in Table IV the N4LO contribution of the currents for the JLab-Pisa group power counting.

TABLE IV. The same as Table III for the JLab-Pisa group power counting scheme of the electroweak currents. For completeness we report also the contributions at N4LO derived by our group. Abbreviations: 1b, one-body; OPE, one-pion exchange; CT, contact terms; TPE, two-pion exchange; NR, nonrelativistic; RC, relativistic corrections; OPE- Δ , one-pion-exchange currents with an intermediate Δ -isobar excitation; and sub, subleading. With the asterisk we indicate the terms that do not appear for the EMN interactions. The term with the superscript A are not yet available for the NV interactions. The dagger indicates that the LECs appearing in these terms have not been determined yet. Note that we explicitly show for each term the LECs that have been fitted on electroweak processes.

Oper.	LO (Q^{-3})	NLO (Q^{-2})	N2LO (Q^{-1})	N3LO (Q^0)	N4LO (Q^1)
$\rho(A)$	—	1b(NR)	OPE	—	TPE ^A CT [†]
$j(A)$	1b(NR)	—	1b(RC) OPE- Δ^*	CT(d_R) OPE	TPE OPE(sub)
$\rho(V)$	1b(NR)	—	1b(RC)	OPE(RC)	TPE
$j(V)$	—	1b(NR)	OPE	1b(RC) OPE- Δ^*	TPE OPE(d_2^V, d_3^V, d_2^S) CT(d_1^V, d_1^S)

IV. ANALYSIS OF THE THEORETICAL UNCERTAINTIES

In this section we focus on the sources of uncertainties and on how we dealt with them. The sources of uncertainties that we consider are four: (i) the uncertainties on the LECs appearing in the nuclear electroweak currents as they result from the fitting procedure and on the single-nucleon axial form factor, (ii) the error due to the truncation of the chiral expansion of the current, (iii) the error due to the truncation of the chiral expansion of the interaction, and (iv) the dependence on the nuclear interaction model. Clearly, also the LECs fitted in the nuclear interaction have an impact on the determination of the full uncertainties as well. However, a comparison of the results obtained with different nuclear interactions as in point (iv) can partially give an estimate of this impact. We are going to consider point (iv) in Sec. V where we will combine the results obtained in for the single interactions. Note also that the four sources of uncertainty are not necessarily independent. However, in this work we treat them as if they were. Moreover, the power counting used for organizing the current terms plays a crucial role in the final determination of the uncertainty. While this cannot be considered as a source of error itself, we computed the uncertainties on the currents considering both available power countings in order to give the most comprehensive picture of the present theoretical situation.

In Table V we present the computed total capture rate for the hyperfine state 1/2 for the various nuclear interactions considered together with the error associated with the various sources of uncertainty considering the Bochum and JLab-Pisa group power counting, respectively. In the table we report the results of the EMN considering the interaction at N3LO. Since the N4LO currents are not fully determined, we performed our analysis considering the currents only up to N3LO using the value of d_R fitted consistently at N3LO as well. We discuss in detail in the following subsections all the various sources of uncertainties. In Table V we present also the results (without errors) for the capture rate in the hyperfine state 3/2. These are consistent with the results of Ref. [15] once the extra contribution of the partial waves $J = 3$ and $J = 4$ is removed ($\approx 0.75\%$).

A. Current LECs uncertainties

The axial nuclear charge and current operators are multiplied by the single-nucleon axial form factor $g_A(q^2)$, with q indicating the four-momentum transfer. The single-nucleon axial form factor can be parametrized as

$$g_A(q^2) = g_A \left(1 - \frac{1}{6} r_A^2 q^2\right), \quad (3.1)$$

where $g_A = 1.2723$ [32] for the NV interactions and $g_A = 1.2754$ [33] for the EMN interactions, and we adopted $r_A^2 = 0.46(16) \text{ fm}^2$, as suggested in Ref. [14]. Since q^2 for the muon capture on deuteron is quite large, the uncertainty on r_A^2 makes a significant impact on the capture rate. At the same time, it is important to study the impact of the uncertainty on the LEC d_R on the total capture rate. Such uncertainty is given in Refs. [27] for the NV interactions and Appendix for EMN interactions. The errors on r_A^2 and d_R have been propagated with standard error propagation techniques, i.e.,

$$\sigma_{\text{LECs}}^2 = \left(\frac{\partial \Gamma}{\partial r_A^2}\right)^2 \sigma^2(r_A^2) + \left(\frac{\partial \Gamma}{\partial d_R}\right)^2 \sigma^2(d_R). \quad (3.2)$$

The 68% confidence level (CL) results can be found in Table V. The computed uncertainties are identical within the showed digits for all the nuclear interactions considered. The reason is that the values of the derivatives in Eq. (3.2) are constant and almost independent of the interactions ($\partial \Gamma / \partial r_A^2 = -24 \text{ s}^{-1} \text{ fm}^{-2}$ and $\partial \Gamma / \partial d_R = 0.66 \text{ s}^{-1}$). The uncertainty we obtain is slightly smaller respect to Ref. [15] (4.4 s^{-1}). This is due to the fact the single-nucleon axial form factor is associated to each term in our axial current and charge operators, while in Ref. [15] it appears only at LO. This slightly reduce the absolute value of the derivative respect to r_A^2 in Eq. (3.2) and therefore the error associated with it. For example, removing the axial form factor from the higher-order terms in the current using the NV1a interaction, we obtain an error of 4.3 s^{-1} consistent with Ref. [15].

The impact of the d_R error on σ_{LECs} is of the order of 1% and therefore completely negligible. This is a consequence of the small contribution that the contact term of the axial current at N3LO gives to the total muon capture. We also tested the impact of the errors on the LECs appearing at N4LO in the

TABLE V. Total muon capture rate on deuteron for all the interactions considered in this work. With $\Gamma^{1/2(3/2)}(J \leq 4)$ we indicate the computed value using the currents and the interactions at N3LO with partial waves up to $J = 4$ in the singlet (triplet) hyperfine state. $\sigma_{k=3(4)}^{C(I)}$ is the standard deviation of the truncation error computed using the Bayesian framework of Ref. [17] for the current (interaction). For the truncation error associated to the current we report the values obtained using both the Bochum group (BPC) and the JLab-Pisa group power counting (JPPC). The values between parenthesis in the fifth, sixth, and seventh columns are the ones obtained using the prescription of Ref. [31]. Finally in the eighth column we report the error computed propagating the uncertainties associated with the LECs appearing in the currents. All the uncertainties are reported at 68% confidence level (CL). The star on the truncation error indicates that the emulator failed the statistic tests for some specific cases (see text for more details).

Name	Pot.	Curr.	$\Gamma^{1/2}$	$\sigma_{k=3}^C$ [BPPC]	$\sigma_{k=3}^C$ [JPPC]	$\sigma_{k=4}^I$	σ_{LECs}	$\Gamma^{3/2}$
NVIa	N3LO	N3LO	393.5	5.1*(3.0)	1.1(0.7)	n.a.	3.9	13.3
NVIb	N3LO	N3LO	393.7	5.1(3.0)	1.1(0.7)	n.a.	3.9	13.5
NVIIa	N3LO	N3LO	392.5	5.1(3.0)	1.1*(0.7)	n.a.	3.9	13.3
NVIIb	N3LO	N3LO	392.6	5.1(3.0)	1.1(0.7)	n.a.	3.9	13.3
EMN450	N3LO	N3LO	396.0	6.4(3.1)	2.2(0.7)	0.3*(0.2)	3.9	13.7
EMN500	N3LO	N3LO	397.3	6.0(3.1)	2.2*(0.7)	0.3*(0.2)	3.9	13.8
EMN550	N3LO	N3LO	397.0	6.2(3.1)	2.1*(0.7)	0.4*(0.2)	3.9	13.8

vector part of the current (see Table IV) obtaining results similar to d_R .

B. Bayesian analysis of truncation error

The analysis of the uncertainties due to the truncation of the chiral expansion for currents and interactions is performed using the `gsum` package² within the formalism introduced by Melendez *et al.* in Ref. [17]. We first review the fundamental points of the Bayesian analysis needed to present our specific case.

1. Brief introduction

We introduce here the main concepts used in our Bayesian analysis of the truncation error in χ EFT. We will refer to Ref. [17] for all the remaining theoretical and technical details behind the analysis. Note that we assume that the chiral expansions of the currents and the interactions are independent. Therefore, we are going to study them separately, keeping fix the interaction order at N3LO when we study the truncation error of the current expansion. In order to study the truncation error of the chiral interaction expansion, we keep the order of the chiral current fixed at N3LO when the interaction order is N2LO and N3LO and at N2LO when the interaction is used at LO and NLO. This choice is made because d_R is not defined for the interaction at LO and NLO. We are going to indicate with a superscript $C(I)$ the specific quantities that are relative to the analysis of the truncation error of the current (interaction). The equation where these indexes are missing are valid for both the cases.

The observable we consider for this analysis is the differential radiative capture $\Gamma(E'_1)$ defined in Eq. (2.7) which depends on the kinetic energy of the neutron E'_1 . This is directly connected with the neutron momentum $p_1 = \sqrt{E_1'^2 + 2E_1'm_n}$, which we are using as independent variable (see Ref. [17]).

For notation clarity in the next two subsections we are going to write the quantity Γ as function of the momentum of the neutron p_1 only.

The k th order EFT prediction can be written as

$$\Gamma_k(p_1) = \Gamma_{\text{ref}}(p_1) \sum_{n=0}^k c_n(p_1) Q^n(p_1), \quad (3.3)$$

where $\Gamma_{\text{ref}}(p_1)$ is a dimension-full overall scale that is selected such that the dimensionless coefficients c_n are of order 1. As in Ref. [17] we take

$$Q(p_1) = \frac{1}{\Lambda_b} \frac{p_1^8 + m_\pi^8}{p_1^7 + m_\pi^7}, \quad (3.4)$$

with m_π the mass of the pion and Λ_b the breakdown scale of the theory. In this work we follow Refs. [17,34] taking $\Lambda_b = 600$ MeV, which is a reasonable value between the cutoffs of the interactions and the formal breaking scale energy of chiral effective field theory (i.e., 1 GeV). The EFT truncation error is then defined as

$$\delta\Gamma_k(p_1) = \Gamma_{\text{ref}}(p_1) \sum_{n=k+1}^{\infty} c_n(p_1) Q^n(p_1). \quad (3.5)$$

Our goal is then to determine this truncation error and the uncertainty associated with it.

The idea of Ref. [17] is to build a stochastic representation of the $c_n(p_1)$ based on a Gaussian process (GP) that emulates our order-by-order chiral calculation. The GP is then exploited to emulate the missing c_n that appears in the EFT truncation error. The basic assumption is that $c_n(p_1)$ are identical independent draws of an underlying GP, i.e.,

$$c_n(p_1) | \mu, \bar{c}^2, \ell \approx^{\text{iid}} \mathcal{GP}[\mu, \bar{c}^2 r(p_1, \bar{p}_1; \ell)], \quad (3.6)$$

where this is specified by the mean μ , the variance \bar{c}^2 , and the correlation length ℓ . The correlation function $r(p_1, \bar{p}_1; \ell)$ is assumed to have an exponential-squared form (see Ref. [17]). The GP hyperparameters μ , \bar{c}^2 , and ℓ are then learned from the training data set which contains order-by-order EFT

²Some of the libraries were slightly modified for addressing the p dependence when computing the truncation error.

calculations. The truncation error distribution is then given by [17]

$$\delta\Gamma_k(p_1)|\mu, \bar{c}^2, \ell, \Lambda_b \approx \mathcal{GP}[m_k(p_1), \bar{c}^2 R_k(p_1, \bar{p}_1; \ell)], \quad (3.7)$$

where

$$m_k(p_1) = \Gamma_{\text{ref}}(p_1) \frac{Q(p_1)^{k+1}}{1 - Q(p_1)}, \quad (3.8)$$

and

$$R_k(p_1, \bar{p}_1; \ell) = \Gamma_{\text{ref}}(p_1) \Gamma_{\text{ref}}(\bar{p}_1) \times \frac{[Q(p_1)Q(\bar{p}_1)]^{k+1}}{1 - Q(p_1)Q(\bar{p}_1)} r(p_1, \bar{p}_1; \ell). \quad (3.9)$$

Note that in Eq. (3.7) we assume that the truncation error distribution depends only on Λ_b and not on the choice of the functional form of $Q(p_1)$ which we assume fixed. The distribution for the full observable will have then mean and covariance respectively given by

$$\Gamma_{\text{th}}(p_1) = \Gamma_k(p_1) + m_k(p_1) \quad (3.10)$$

and

$$\Sigma_{\text{th}}(p_1, \bar{p}_1, \ell) = \bar{c}^2 R_k(p_1, \bar{p}_1; \ell). \quad (3.11)$$

Finally, the total capture rate is the integral of $\Gamma(p_1)$ on p_1 (this can be directly derived from Eq. (2.7) after changing variables). For all practical purposes this integral can be written as a discrete sum over M points, i.e.,

$$\Gamma_{\text{th}} = \sum_{i=1, M} \omega_i \Gamma_{\text{th}}(p_1(i)), \quad (3.12)$$

where ω_i are the specific weights of the chosen integration method. From Eq. (3.12) it follows immediately that $\Gamma_{\text{th}} = \Gamma_k + \delta\Gamma_k$, with $\Gamma_k(\delta\Gamma_k)$ the integration over p_1 of $\Gamma_k(p_1)(\delta\Gamma_k(p_1))$. What we want is then to find the distribution of

$$\delta\Gamma_k = \sum_{i=1, M} \omega_i \delta\Gamma_k(p_1(i)). \quad (3.13)$$

Using the properties of Gaussian random variables we find

$$\delta\Gamma_k|\mu, \bar{c}^2, \ell, \Lambda_b \approx \mathcal{N}[M_k(\mu), \sigma_k^2(\bar{c}^2, \ell, \Lambda_b)], \quad (3.14)$$

where \mathcal{N} indicates the normal distribution and

$$M_k(\mu) = \sum_{i=1, M} \omega_i m_k(p_1(i)) \quad (3.15)$$

and

$$\sigma_k^2(\bar{c}^2, \ell, \Lambda_b) = \bar{c}^2 \sum_{i, j=1, M} \omega_i \omega_j R_k(p_1(i), p_1(j); \ell). \quad (3.16)$$

Note that Eq. (3.14) is no longer a Gaussian process since we now have a single random variable. With this final equation we can discuss the specific details of our analysis.

2. Currents truncation errors

For the analysis of the truncation error of the chiral expansion of the currents we consider the factorization

$$\Gamma_k^C(p_1) = \Gamma_{\text{ref}}^C(p_1) \sum_n c_n^C(p_1) Q^n(p_1), \quad (3.17)$$

where $Q^n(p_1)$ has been defined in Eq. (3.4), $n = \{0, 2, 3\}$ for the Bochum group power counting and $n = \{0, 1, 2, 3\}$ for the JLab-Pisa one, and we select the reference scale as

$$\Gamma_{\text{ref}}^C(p_1) = \frac{\Gamma_{\text{LO}}^C(p_1) Q^{-3}(p_1)}{10}. \quad (3.18)$$

In such a way we reconstruct the correct power of $Q(p_1)$, such that the calculation does not suffer of inversion problems, and the $c_n^C(p_1)$ are naturally sized (this is the reason for the factor 1/10). We remove from the analysis the coefficient $c_0^C(p_1)$ because the choice of the reference value makes it not significant for training the emulator.

We decide to limit our analysis up to $p_1^{\text{max}} = 195$ MeV. This permits us to verify the hypothesis that the $c_n^C(p_1)$ are distributed as in Eq. (3.7) using the diagnostics presented in Ref. [17]. Beyond p_1^{max} the coefficients $c_n^C(p_1)$ become very large and the hypothesis of Eq. (3.7) is no longer statistically valid. The most reasonable explanation is the fact that the scale Q in Eq. (3.4) is not the proper one for this process at such large p_1 . Note that the contribution to the total capture rate of the tail beyond p_1^{max} is $\lesssim 2 \text{ s}^{-1}$. Therefore, the impact on the error computation is minimal.

The data set generated using the Bochum group power counting consists of 195 data points on a grid that starts from zero and has a step of 1 MeV. For training the emulator we use 4(5) data points distant 50(40) MeV for the NV(EMN) interactions. We used more points in the EMN case because of the larger oscillations of the coefficients as function of p_1 . As validation set we used 13 data points distant 15 MeV one from each other. More data points in the validation data set give rise to ill-defined covariance matrices. Finally, we use 10^{-4} as the value for the variance of the white noise needed to stabilize the matrix inversion (i.e., the nugget). Smaller values generate instabilities in the inversion of the covariance matrices, while values larger than 10^{-3} generate too much noise in the final results.

In Fig. 1(a) we report the value of the coefficients $c_n^C(p_1)$ together with the GP emulator results and their 2σ interval for the EMN550 interaction using the Bochum power counting. From a first inspection, the GP emulator is able to nicely reproduce the χEFT calculation. To assess quantitatively the quality of the emulation we performed the Mahalanobis distance (D_{MD}^2) test presented in Fig. 1(b) and the pivoted Cholesky decomposition (D_{PC}) test presented in Fig. 1(c). The Mahalanobis distance test is a generalization of the squared residuals in the case of correlated data points (see Ref. [17] for more details). The comparison with the reference χ^2 distribution shows a compatibility of the emulation with the data points within the 95% CL (whiskers) for both c_2^C and c_3^C . This is evident also at the level of the more informative Cholesky decomposition (see Ref. [17]). The validation points are distributed almost uniformly within 1σ , with only a few points close to the 2σ line. Similar results on the two diagnostics are obtained for all the other interactions, except for the NV1a model. In this case, the casual cancellation of the current contributions at N3LO give rise to coefficients c_3^C practically zero. Therefore, almost no stochastic fluctuations are generated in the emulator. This gives rise to an anomalous coincidence among the emulator and the simulator results,

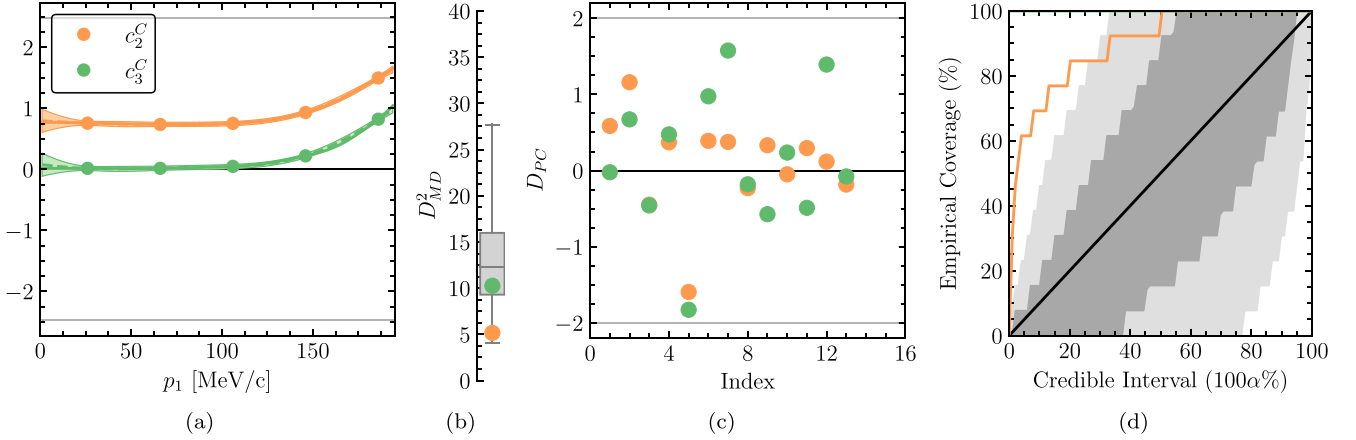


FIG. 1. The Gaussian process modeling of the current chiral expansion coefficients and its diagnostics for the EMN550 interaction using the Bochum power counting. (a) The simulators (solid lines, i.e., our calculation) along with the corresponding Gaussian process emulators (dashed lines) and their 2σ intervals (bands). The data used for training are denoted by dots. (b) The Mahalanobis distances compared to the mean (interior line), 50% (box), and 95% (whiskers) credible intervals of the reference distribution. (c) The pivoted Cholesky diagnostics versus the index along with 95% credible intervals (gray lines). (d) The credible interval diagnostics for the truncation error bands. The $1(2)\sigma$ is represented with the dark (light) gray band. The steepness of the orange line indicates that the N2LO and the N3LO are very close to each other (see text for more details).

making the emulator fail the Mahalanobis and the pivoted Cholesky test for the NVIa interaction (i.e., the simulator seems to work statistically too good). The final error is in any case in reasonable agreement with the others and we report in Table VI with a star.

In the credible interval diagnostic showed in Fig. 1(d) we study if the truncation error computed at each order is compatible with the correction at the next order within a certain CL. The CL bands are constructed by sampling a large number of emulators (1000) from the underlying process. The credible intervals are then plotted against the percentage of validation points found within the interval, i.e., if the emulator contains only a small amount of the validation points is overconfident (in the figure represented as horizontal lines) and in the other case is underconfident (vertical lines). The orange line in Fig. 1(d) is the credible interval for $\Delta\Gamma_2^C(p_1) = \Gamma_2^C(p_1) - \Gamma_3^C(p_1)$ compared with the reference distribution of $\Delta\Gamma_2^C(p_1)$, which is also the only one we can compute performing this analysis. The credible interval for $\Delta\Gamma_2^C(p_1)$ shows us that the emulation is in general underconfident. That is understandable since the differences among the simulated spectra at N2LO and N3LO is minimal (see Fig. 3). The

results for the confidence interval diagnostics of the other interactions are practically identical.

A similar analysis has been performed considering the data generated using the JLab-Pisa power counting for the NV(EMN) interaction up to 195(190) MeV with 1 MeV step. For training the emulator we use 5 data points distant 35(40) MeV. As validation set we used 13 data points distant 15 MeV one from each other. The nugget we use is $10^{-4}(2 \times 10^{-4})$.

The results for the diagnostic of the EMN550 interaction are shown in Fig. 2. Again the emulator seems able to reproduce nicely the coefficients $c_n^C(p_1)$. However, the emulator starts to have difficulties for $p_1 > 150$ MeV, since the coefficients $c_n(p_1)$ become very stiff, especially c_3^C [see Fig. 2(a)]. Consequently, the Mahalanobis distance test is slightly failed by the emulator for the coefficient c_3^C [Fig. 2(b)]. This is confirmed also by the pivoted Cholesky test where several blue points are out of the 2σ range [Fig. 2(c)]. Note also the statistically anomalous coincidence of the emulator with the simulator for the coefficients c_1^C . The analysis of the EMN500 interaction give almost identical results, while for the EMN450 the emulator pass all the tests including the c_3^C coefficient. For the NV interaction the emulator pass all the tests again except in the case of the c_3^C coefficient for the NVIIa interaction that present rather strong oscillation that the emulator is not able to address completely.

In Fig. 2(d) we show the credible interval for $\Delta\Gamma_1^C(p_1) = \Gamma_1^C(p_1) - \Gamma_2^C(p_1)$ (green) and $\Delta\Gamma_2^C(p_1) = \Gamma_2^C(p_1) - \Gamma_3^C(p_1)$ (orange) compared with the reference distribution. The vertical behavior for both cases indicate that the emulator is underconfident, i.e., the error estimated is statistically larger than expected. This indicate also that the error generated at given order contain the result at next order. Even if the emulator is not able to describe all the features of the coefficients c_n^C , the truncation error estimate is reliable even if rather conservative.

TABLE VI. Absolute and relative contributions to the estimated total theoretical error from the various uncertainty sources for both the Bochum (BPC) and JLab-Pisa (JPPC) power counting.

Uncertainty source	BPC	JPPC
r_A^2	5.6(30.8%)	5.4(75.2%)
Other current LECs	Negligible	
χ EFT truncation–currents	8.1(65.2%)	2.4(14.6%)
χ EFT truncation–interactions	0.5(0.3%)	0.5(0.7%)
Model dependence	1.9(3.7%)	1.9(9.5%)

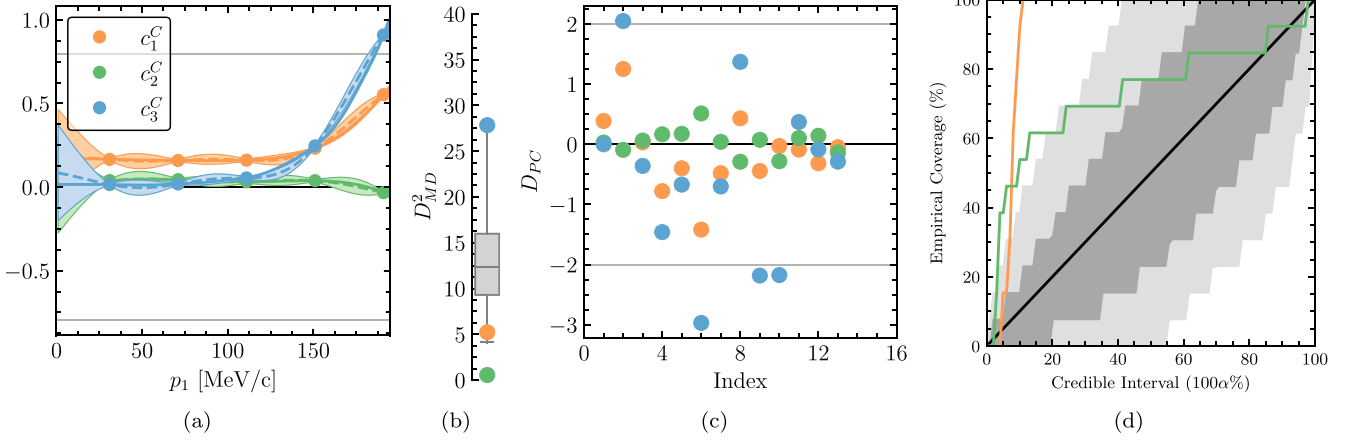


FIG. 2. Same as Fig. 1 for the EMN550 interaction using the JLab-Pisa power counting.

The diagnostic gave us an overall good result on the quality of the GP emulation. We computed then the truncation error using Eq. (3.7). The order-by-order spectra obtained from the EMN550 interaction with 95% CL truncation error for both the Bochum and JLab-Pisa power counting are shown in Fig. 3 and Fig. 4, respectively. Finally, we compute the truncation error on the total capture rate as in Eq. (3.16) for each interaction. The 68% CL results are reported in Table V. Note that the integration has been performed only up to $p_1^{\max} = 195$ MeV. In order to estimate the error arising from the remaining part of the spectra we used the Epelbaum *et al.* prescription (EP) [31] as considered in Ref. [16]. By doing so, we have found that the contribution to the total truncation error of this part of the spectra is completely negligible. Similar results have been obtained for all the other interactions.

In Table V we report between parentheses also the errors computed on the total capture rate using the EP exactly as in Ref. [16]. To give a more statistical insight, we assume that the expected decay rate is uniformly distributed within the limits settled by the extreme values and so the 68% CL is given by the value of the truncation error divided by $\sqrt{3}$. As it can be seen from the table, in general the error estimated with the EP is smaller than the one obtained using the Bayesian analysis.

3. Interaction truncation error

The other source of uncertainties we treat with the Bayesian analysis is the one arising from the truncation of the nuclear interaction chiral expansion. Unfortunately, we do not have all the orders of the NV interactions. Therefore, we limit the analysis only to the EMN interaction family.

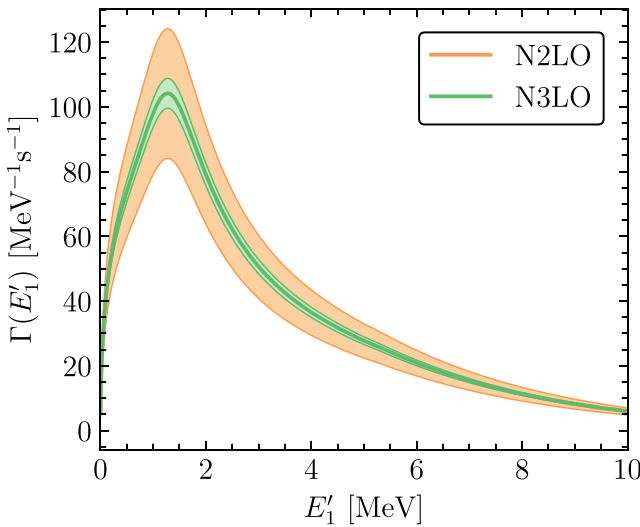


FIG. 3. The differential capture rate as function of the neutron energy E_1' computed with the EMN550 interaction fixed at N3LO for various order of the current N2LO (orange) and N3LO (green) using the Bochum power counting. The bands represent the 2σ truncation errors at each order.

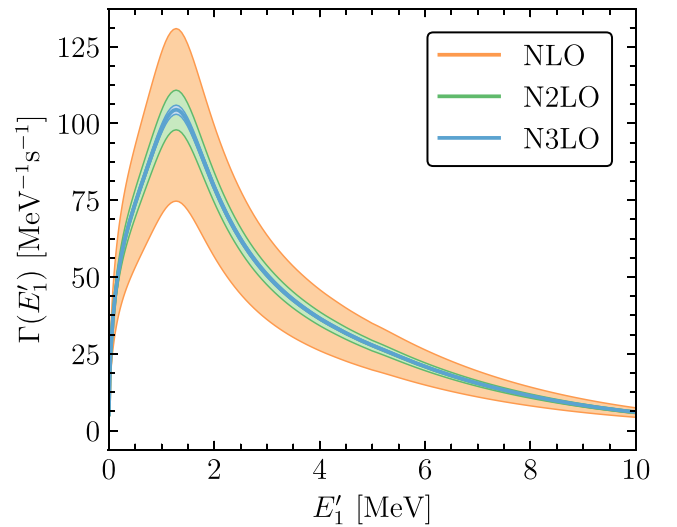


FIG. 4. The differential capture rate as function of the neutron energy E_1' computed with the EMN550 interaction fixed at N3LO for various order of the current NLO (orange), N2LO (green), and N3LO (blue) using the JLab-Pisa power counting. The bands represent the 2σ truncation errors at each order.

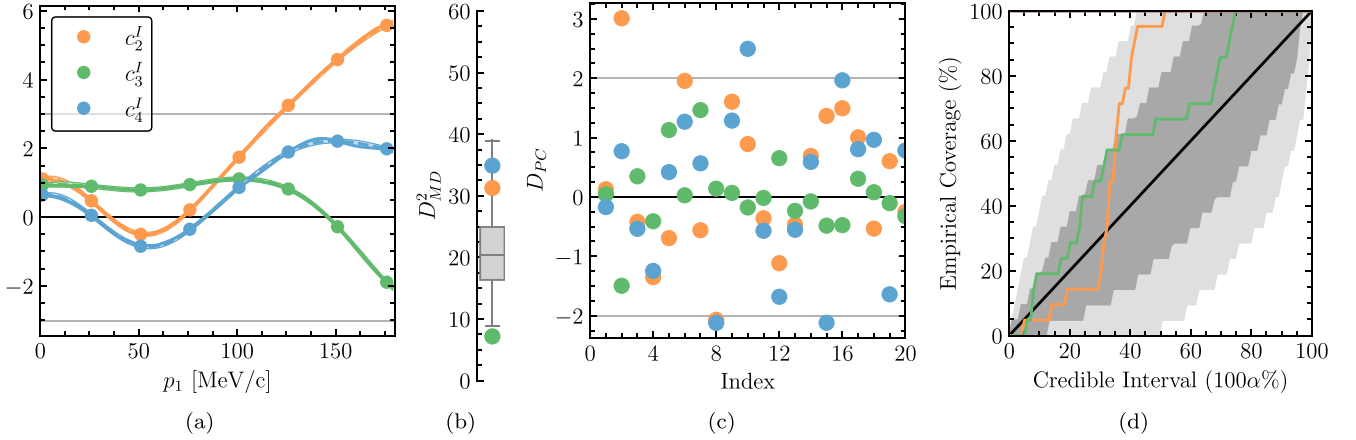


FIG. 5. Same as Fig. 1 but for the truncation errors of the interaction chiral expansion. The results reported in the figure are obtained using the EMN550 interaction fixing the order of the chiral current at N2LO for the interaction at NLO, and at N3LO in the remaining cases.

The procedure that we use is identical to the one used in the analysis of the current truncation errors. The main difference is in the factorization we use, chosen to be

$$\Gamma_k^I(p_1) = \Gamma_{\text{ref}}^I(p_1) \sum_{n=0,2,3,4} c_n^I(p_1) Q^n(p_1), \quad (3.19)$$

where $Q^n(p_1)$ has been defined in Eq. (3.4) and $\Gamma_{\text{ref}}^I(p_1) = \Gamma_{\text{LO}}^I(p_1)$. This choice of the reference value makes the coefficient c_0^I useless for training the emulator since it results identical to one. Therefore we exclude it in our analysis. A similar choice was done in Refs. [17,34].

To obtain a reasonable result for the GP emulator we restrict the momentum range of the analysis to 180 MeV. For training the emulator we use 8 points distant 25 MeV and we take 21 test points 8 MeV apart from each other. The nugget we used in this case is 2×10^{-4} . Note that we need a higher density of training points compared to the currents because of the large oscillations of the coefficients c_n^I .

In Figs. 5 we present the results of the emulation together with the diagnostic performed to verify the quality of the emulation trained on the EMN550 interaction model results. As it can be observed from the figure, the Mahalanobis distance [Fig. 5(a)] and the coefficient c_3^I show a slightly anomalous coincidence among the simulator and the emulator, confirmed by a high density of green points close to zero in the Cholesky decomposition [Fig. 5(b)]. A similar behavior is present for the coefficient c_4^I in the case of the EMN500 interaction. For the EMN450 the emulator fails the Mahalanobis distance test for the c_4^I as well. In this case the reason is the large oscillation of this coefficient at large momentum p_1 that makes the emulator very hard to train.

In order to check if we could improve the emulation, we performed several other tests changing the parameters of the analyses without finding any significant improvement on the statistical tests. Despite this, the truncation errors obtained with these other analysis are numerically identical to the one obtained using the parameters shown in the text.

On the other hand, the credible interval diagnostic test (Fig. 5) for all the EMN interactions a compatibility of more

than 95% between the truncation error at given order and the prediction at the next one up to N3LO over all the empirical coverage. This indicates that at each order the estimated error contains the next order correction. Therefore, despite the emulator is not able to pass the statistical tests for each c_n^I , the estimate of the truncation error seems to be reliable. We present in Fig. 6 the differential capture rate spectrum computed order by order with the relative truncation error for the EMN550 interaction. The truncation error on the total capture rate obtained using Eq. (3.16) has been reported in Table V. Once again we have verified, using the EP, that the error arising from the tail of the spectra not analyzed in the Bayesian procedure is negligible. The error obtained applying

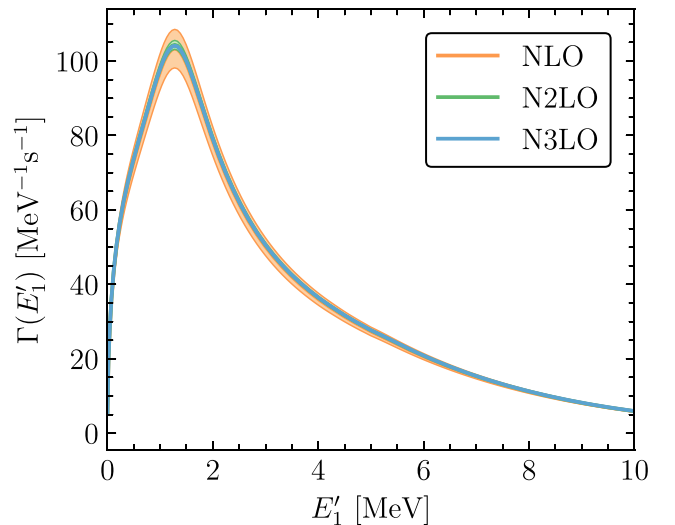


FIG. 6. The differential capture rate as function of the neutron energy E'_1 computed with the EMN550 interaction at NLO (orange), N2LO (green), and N3LO (blue). The bands represent the 2σ truncation errors at each order. Note that the chiral order of the current used in this analysis is N2LO when the interaction is at NLO and N3LO in the rest of the cases.

the EP over all the spectrum can be found in Table V between parentheses.

4. Discussion

Before concluding this section some remarks are in order.

- (i) The power counting of the currents has a major impact on the determination of the truncation errors. As can be seen from our results the Bochum group power counting gives larger error bands than the JLab-Pisa. This has been seen already in Ref. [35] for the electromagnetic terms of the current.
- (ii) Even if the results for all the interactions are compatible within the error bars, the capture rates obtained using the local interactions are systematically lower than the ones obtained using the nonlocal interactions. This is partially due to the different sign of the contact terms in the axial current at N3LO.
- (iii) In this work we chose to study separately the truncation error associated to the interaction and the currents. Clearly this is not completely correct because of precise relations between the Hamiltonian and the currents such as current conservation. Even if such relations exist, they are not completely fulfilled order by order by the available currents yet. We did some attempt to compute the truncation errors for the Hamiltonian and the currents together. However, we did not find any benefit for the analysis, obtaining on the other side an error typically smaller than the current truncation error reported here. Therefore we decided to consider here the most conservative approach.

V. FINAL RESULTS AND DISCUSSION

We consider now the last source of uncertainty, i.e., the one arising from model dependence. Compared with previous studies, where essentially a reference value was obtained as the mean over all the interactions considered and the error was estimated as the difference between the extreme cases, we follow a slightly different approach as proposed in Ref. [36] and often used in lattice QCD for model averaging.

We take for each of the model as our best estimate of the total capture rate the one computed, i.e., we assume

$$\Gamma_i(\infty) = \Gamma_i(\text{comp}), \quad (4.1)$$

where i indicate the model used in the calculation. We consider the worst scenario in which all the three sources of error are fully correlated and so the total error is given by

$$\sigma_i = \sigma_{i,k=3}^C + \sigma_{i,k=4}^I + \sigma_{i,\text{LECS}}. \quad (4.2)$$

Note that as $\sigma_{i,k=3}^C$ we consider only the one obtained using the Bochum power counting that represent the worst-case scenario. For the NV interaction family we take $\sigma_{k=4}^I = 0.4 \text{ s}^{-1}$ as in the worst case of the EMN interactions.

Following Ref. [36] the average of the models is given by

$$\langle \Gamma \rangle = \sum_i \Gamma_i \text{pr}(i), \quad (4.3)$$

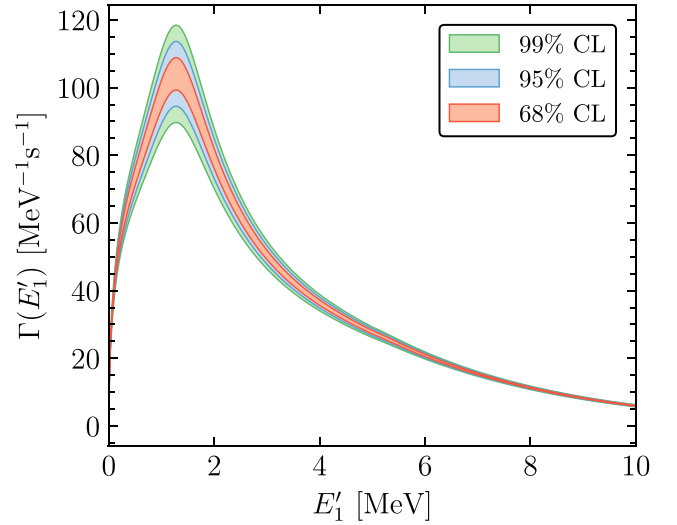


FIG. 7. The recommended differential capture rate as function of the kinetic neutron energy E'_1 . The green, blue, and red bands represent respectively the 99%, 95%, and 68% CL. Note that the difference among the bands can be appreciated only at the peak of the spectra.

while the variance can be written as

$$\sigma_\Gamma^2 = \sum_i \sigma_i^2 \text{pr}(i) + \sigma_{\Gamma,\text{syst}}^2, \quad (4.4)$$

with the systematic error given by the model dependence obtained as

$$\sigma_{\Gamma,\text{syst}}^2 = \sum_i \Gamma_i^2 \text{pr}(i) - \left[\sum_i \Gamma_i \text{pr}(i) \right]^2. \quad (4.5)$$

In these equations, with “pr” we have indicated the probability of a certain model. Since there is no reason to privilege local or nonlocal interactions, and no reason to privilege any interaction within a given class, we assign the following probabilities:

$$\text{pr}(i) = \begin{cases} \frac{1}{8}, & \text{if } i \text{ local} \\ \frac{1}{6}, & \text{if } i \text{ nonlocal} \end{cases}. \quad (4.6)$$

Using the Bochum group power counting we obtain

$$\Gamma_{\text{th}}(\text{BPC}) = (395 \pm 10) \text{ s}^{-1} \quad (68\% \text{CL}), \quad (4.7)$$

while using the JLab-Pisa power counting

$$\Gamma_{\text{th}}(\text{JPPC}) = (395 \pm 6) \text{ s}^{-1} \quad (68\% \text{CL}). \quad (4.8)$$

As recommended value we select the more conservative result obtained using the Bochum group power counting.

An identical analysis have been performed on the differential capture rate for each value of E'_1 . Our recommended spectra obtained using the Bochum group power counting is shown in Fig. 7 with the bands at 68%, 95%, and 99% CLs. A table with the numerical values of these final spectra is provided as supplementary material [37].

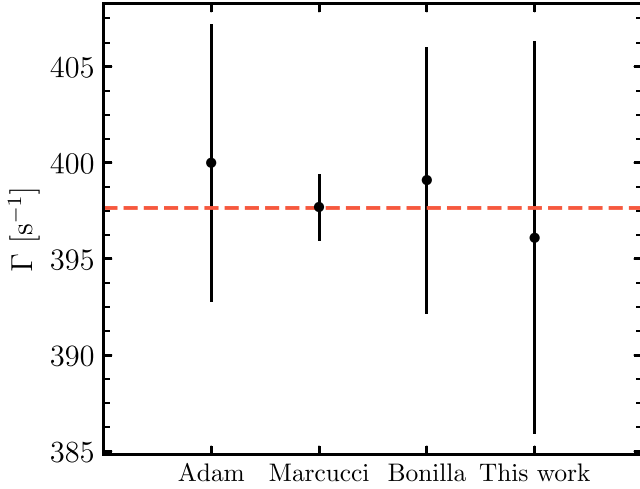


FIG. 8. Comparison of the theoretical results obtained in our work using the Bochum (BPC) and JLab-Pisa (JPPC) power counting with the χ EFT results of Refs. [10,11,15]. The errors in the previous works have been assumed to be the limit of a uniform distribution and then divided by $\sqrt{3}$ to obtain the 68% CL. Note that only in Ref. [15] and in the present work various sources of uncertainty besides the model dependence were considered. The red dashed line represent the arithmetic mean of all the theoretical results.

The comparison of our results with those present in the literature still obtained within χ EFT can be seen in Fig. 8.³ For the calculations in Refs. [10,15] we have assumed that the errors represent the extreme of a uniform distribution. For Ref. [11], we have considered as limit of the distribution the minimal and the maximal reported results. Therefore, in Fig. 8 we report the error divided for $\sqrt{3}$, in order to obtain the 68% CL. Note also that only in our work and in Ref. [15] the error includes the uncertainty on r_A^2 .

The capture rates obtained in this work using the local interactions are systematically smaller than the ones obtained using the nonlocal ones. Therefore, the overall result is slightly smaller compared with the world literature in which only nonlocal chiral interactions have been used. On the other hand, all the theoretical χ EFT calculations are consistent within 1σ . We do not proceed in comparing our results with the available experimental data of Refs. [1–4] because of their large uncertainties.

In order to appreciate the importance of the various uncertainty sources in the total error budget, we list in Table VI their absolute and relative weight in percentage for the two considered power counting. In the JLab-Pisa power counting the main source of uncertainty results r_A^2 while in the case of the Bochum power counting the current truncation error become the dominant source. The model dependence slightly increases the total error but it is smaller than the error generated by the current truncation error and r_A^2 . Note that the truncation error obtained here using the Bochum power counting is similar to truncation error estimated in Ref. [15],

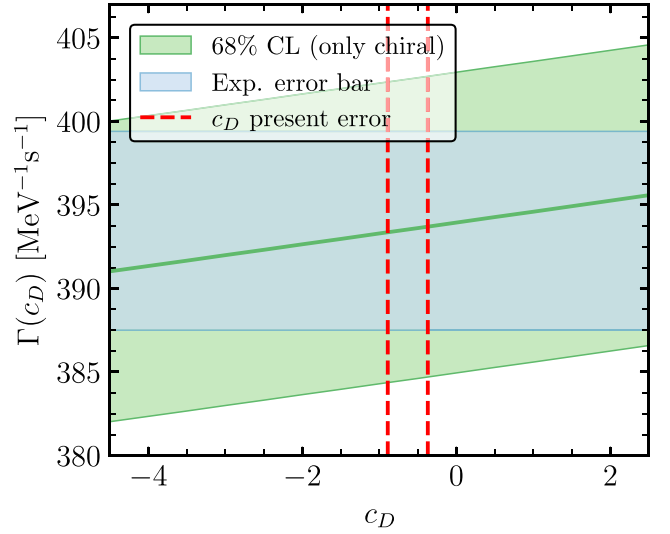


FIG. 9. Capture rate as function of the value of c_D for the NV1a interaction. The green band represent the error on $\Gamma^{3/2}$ due to the truncation error on the chiral expansion of the current and the interaction. The red dashed lines represent the present error bar on c_D . The blue horizontal line is the error band corresponding to a hypothetical result of MuSun $\Gamma^{3/2} = 393.5 \text{ s}^{-1}$ with a 1.5% total error.

using the prescription of Ref. [38], once properly rescaled for the different value of Λ_b used in our work.

We want to underline that reducing the uncertainty on r_A^2 is crucial for testing pure χ EFT effects on the muon capture on deuteron at a few-percentages level. In this sense recent lattice QCD results on the computation of the nucleon axial form factors are extremely encouraging (see Ref. [39] for a review). However, while experimental efforts are on going to reduce the experimental error, improvements on the theoretical side for reducing the truncation errors are crucial to extract physical parameters from this observable.

VI. IMPACT ON THE MUSUN EXPERIMENT

In this section we present a minimal study of the impact of our results in the analysis of the future experimental results of MuSun. For our analysis we assume that the final error of the experiment is the expected precision of $\approx 1.5\%$ [5]. Since this is just a preliminary analysis we consider only the nuclear interaction NV1a and the error associated to this interaction reported in the first line of Table V. For this analysis we assume that the MuSun experiment finds a central value for the total capture rate of 393.5 s^{-1} and an error of 5.9 s^{-1} (1.5%).

First, we study the dependence of the total capture rate as function of the value of the LEC c_D from which d_R depends linearly.

As can be seen in Fig. 9 the dependence of Γ on c_D is linear but with a very small slope. Indeed, just considering only the chiral truncation errors (green band), the experimental value with an uncertainty of $\approx 1.5\%$ (blue horizontal band) would not have any impact on the improvement of the present c_D

³For the Marcucci *et al.* [10] we report the result in the Erratum.

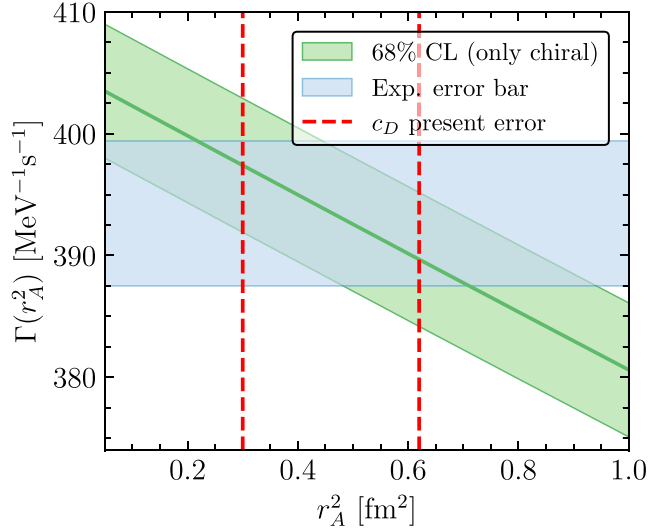


FIG. 10. Capture rate as function of the value of r_A^2 for the NVIA interaction. The green band represent the error on Γ due to the truncation error on the chiral expansion of the current and the interaction. The red dashed lines represent the 68% CL on Γ considering the error on r_A^2 as reported in Ref. [14]. The blue dashed lines represent the predicted 68% CL on Γ with an error of 10% on r_A^2 .

constraints (red vertical dashed lines). Indeed a 1.5% precision on the experimental result corresponds to a very large set of values of c_D , much larger than the present constrains.

We can perform a similar analysis varying r_A^2 . In this case for simplicity we keep c_D fixed. In Fig. 10 we plot the capture rate as function of r_A^2 for the NVIA interaction. The red dashed lines represents the present uncertainty on r_A^2 . The blue band again is the hypothetical result of MuSun with a $\approx 1.5\%$ error. As can be seen, the overlap region of the blue and green bands spans a region of values of r_A^2 much larger than the present limits on it. This indicates that considering our most conservative estimate on the theoretical errors, the MuSun experiment with the present precision goal cannot be a useful source for having an independent estimate of r_A^2 .

Although the present theoretical error bands does not allow, with the expected precision of the MuSun experiment, to obtain new determination of fundamental constants, the MuSun experiment is still a fundamental test for the parameters of chiral effective field theory. Indeed, MuSun will be the first precise measurement of the rate for a weak process in the two-nucleon system, which can be compared with theoretical predictions accompanied by fully quantified uncertainties. Any strong deviation of the experimental results or inconsistency with the present literature would imply the necessity of a profound revision for the chiral electroweak currents. Furthermore, we stress that the MuSun experiment remains one of the best options to access with good accuracy the LEC

TABLE VII. Values for the LECs $c_{1,3,4}$, c_D , and c_E at the chiral orders N2LO, N3LO, and N4LO. The c_D and c_E LECs reproduce the $A = 3$ binding energies and the GT matrix element in tritium β -decay, as explained in the text.

	Λ	c_1	c_3	c_4	c_D	c_E
N2LO	450	-0.74	-3.61	2.44	-0.13(20)	-0.09(4)
N2LO	500	-0.74	-3.61	2.44	-0.86(19)	-0.32(4)
N2LO	550	-0.74	-3.61	2.44	-1.93(20)	-0.73(4)
N3LO	450	-1.07	-5.32	3.56	-0.42(20)	0.06(5)
N3LO	500	-1.07	-5.32	3.56	-2.73(23)	-1.03(5)
N3LO	550	-1.07	-5.32	3.56	-4.35(24)	-2.16(5)
N4LO	450	-1.10	-5.54	4.17	0.17(20)	0.04(5)
N4LO	500	-1.10	-5.54	4.17	-3.02(25)	-1.21(4)
N4LO	550	-1.10	-5.54	4.17	-4.48(24)	-2.35(4)

L_{1A} present (see, for example, the work of Chen *et al.* [40]), within pionless EFT, in several two-nucleon processes, among which, besides muon capture, also the proton-proton fusion reaction, of paramount importance in astrophysics.

ACKNOWLEDGMENTS

The authors thank Professor P. Kammel for critical reading of the paper and helpful suggestions. A.G. thanks Professor D. Phillips for useful discussion on the Bayesian analysis and the use of the gsum package and A. Rodas for the suggestion on the model averaging. We thank the BUQEYE collaboration for making the gsum package available. The calculation was performed using resources of the National Energy Research Scientific Computing Center (NERSC), a U.S. Department of Energy Office of Science User Facility using NERSC Award No. NP-ERCAP0023221.

APPENDIX: FIT OF THE c_D LOW ENERGY CONSTANT FOR THE EMN INTERACTIONS

We updated the fit of the values of the LECs c_D and c_E using the updated value for $g_A = 1.2754$ [33] and the tritium β -decay Gamow-Teller matrix element $GT = 0.9501 \pm 0.0024$ as in Fit-3 of Ref. [41] and also Ref. [42]. Note that we use as definition for d_R

$$d_R = -\frac{M_N}{4\Lambda_\chi g_A} c_D + \frac{1}{3} M_N (c_3 + 2c_4) + \frac{1}{6}, \quad (\text{A1})$$

where M_N is the nucleon mass, g_A the nucleon axial coupling, and c_3, c_4 are LECs with the values listed in the table. We refitted the two LECs using the procedure of Ref. [10], i.e., fixing the LECs c_D and c_E to reproduce the $A = 3$ binding energies and the GT matrix element of tritium β -decay. In Table VII we present the results of the fit together with the values of the LECs $c_{1,3,4}$ used in the currents and the interactions.

[1] I. T. Wang, E. W. Anderson, E. J. Bleser, L. M. Lederman, S. L. Meyer, J. L. Rosen, and J. E. Rothberg, *Phys. Rev.* **139**, B1528 (1965).

[2] A. Bertin, A. Vitale, A. Placci, and E. Zavattini, *Phys. Rev. D* **8**, 3774 (1973).

- [3] G. Bardin, J. Duclos, J. Martino, A. Bertin, M. Capponi, M. Piccinini, and A. Vitale, *Nucl. Phys. A* **453**, 591 (1986).
- [4] M. Cargnelli *et al.*, *Nuclear Weak Process and Nuclear Structure, Yamada Conference XXIII*, edited by M. Morita, H. Ejiri, H. Ohtsubo, and T. Sato (World Scientific, Singapore, 1989), p. 115.
- [5] P. Kammel on behalf of the MuSun collaboration, *SciPost Phys. Proc.* **5**, 018 (2021).
- [6] L. E. Marcucci, *Int. J. Mod. Phys. A* **27**, 1230006 (2012).
- [7] L. E. Marcucci, M. Piarulli, M. Viviani, L. Girlanda, A. Kievsky, S. Rosati, and R. Schiavilla, *Phys. Rev. C* **83**, 014002 (2011).
- [8] J. Golak, R. Skibiński, H. Witała, K. Topolnicki, A. E. Elmeshneb, H. Kamada, A. Nogga, and L. E. Marcucci, *Phys. Rev. C* **90**, 024001 (2014); [**90**, 029904(E) (2014)].
- [9] S. Ando, T.-S. Park, K. Kubodera, and F. Myhrer, *Phys. Lett. B* **533**, 25 (2002).
- [10] L. E. Marcucci, A. Kievsky, S. Rosati, R. Schiavilla, and M. Viviani, *Phys. Rev. Lett.* **108**, 052502 (2012); [**121**, 049901 (2018)].
- [11] J. Adam, M. Tater, E. Truhlik, E. Epelbaum, R. Machleidt, and P. Ricci, *Phys. Lett. B* **709**, 93 (2012).
- [12] L. E. Marcucci, J. Dohet-Eraly, L. Girlanda, A. Gnech, A. Kievsky, and M. Viviani, *Front. Phys.* **8**, 69 (2020).
- [13] B. Acharya, A. Ekström, and L. Platter, *Phys. Rev. C* **98**, 065506 (2018).
- [14] R. J. Hill, P. Kammel, W. J. Marciano, and A. Sirlin, *Rep. Prog. Phys.* **81**, 096301 (2018).
- [15] J. Bonilla, B. Acharya, and L. Platter, *Phys. Rev. C* **107**, 065502 (2023).
- [16] L. Ceccarelli, A. Gnech, L. E. Marcucci, M. Piarulli, and M. Viviani, *Front. Phys.* **10**, 1049919 (2023).
- [17] J. A. Melendez, R. J. Furnstahl, D. R. Phillips, M. T. Prato, and S. Wesolowski, *Phys. Rev. C* **100**, 044001 (2019).
- [18] “Buqeye collaboration” <https://buqeye.github.io/publications/>.
- [19] V. A. Andreev, R. M. Carey, V. A. Ganzha, A. Gardestig, T. P. Goringe, F. Gray, D. W. Hertzog, M. Hildebrandt, P. Kammel, B. Kiburg, S. Knaack, P. Kravtsov, A. Krivshich, K. Kubodera, B. Lauss, K. R. Lynch, E. Maev, O. Maev, F. Mulhauser, F. Myhrer, C. Petitjean, G. E. Petrov, R. Prieels, G. N. Schapkin, G. G. Semenchuk, M. A. Soroka, V. Tishchenko, A. A. Vasilyev, A. Vorobyov, M. Vznuzdaev, and P. Winter, [arXiv:1004.1754](https://arxiv.org/abs/1004.1754).
- [20] W. Kohn, *Phys. Rev.* **74**, 1763 (1948).
- [21] J. Walecka, *Theoretical Nuclear and Subnuclear Physics* (Imperial College Press, London, 1995).
- [22] J. C. Hardy and I. S. Towner, *Phys. Rev. C* **102**, 045501 (2020).
- [23] M. Piarulli, L. Girlanda, R. Schiavilla, R. N. Pérez, J. E. Amaro, and E. R. Arriola, *Phys. Rev. C* **91**, 024003 (2015).
- [24] M. Piarulli, L. Girlanda, R. Schiavilla, A. Kievsky, A. Lovato, L. E. Marcucci, S. C. Pieper, M. Viviani, and R. B. Wiringa, *Phys. Rev. C* **94**, 054007 (2016).
- [25] D. R. Entem, R. Machleidt, and Y. Nosyk, *Phys. Rev. C* **96**, 024004 (2017).
- [26] A. Baroni, L. Girlanda, S. Pastore, R. Schiavilla, and M. Viviani, *Phys. Rev. C* **93**, 015501 (2016).
- [27] A. Baroni, R. Schiavilla, L. E. Marcucci, L. Girlanda, A. Kievsky, A. Lovato, S. Pastore, M. Piarulli, S. C. Pieper, M. Viviani, and R. B. Wiringa, *Phys. Rev. C* **98**, 044003 (2018).
- [28] S. Pastore, L. Girlanda, R. Schiavilla, M. Viviani, and R. B. Wiringa, *Phys. Rev. C* **80**, 034004 (2009).
- [29] M. Piarulli, L. Girlanda, L. E. Marcucci, S. Pastore, R. Schiavilla, and M. Viviani, *Phys. Rev. C* **87**, 014006 (2013).
- [30] H. Krebs, *Eur. Phys. J. A* **56**, 234 (2020).
- [31] E. Epelbaum, H. Krebs, and U.-G. Meissner, *Eur. Phys. J. A* **51**, 53 (2015).
- [32] C. Patrignani, *Chin. Phys. C* **40**, 100001 (2016).
- [33] P. D. Group, P. A. Zyla, R. M. Barnett, J. Beringer, O. Dahl, D. A. Dwyer, D. E. Groom, C.-J. Lin, K. S. Lugovsky, E. Pianori *et al.*, *Progr. Theor. Exp. Phys.* **2020**, 083C01 (2020).
- [34] B. Acharya and S. Bacca, *Phys. Lett. B* **827**, 137011 (2022).
- [35] J. D. Martin, S. J. Novario, D. Lonardonì, J. Carlson, S. Gandolfi, and I. Tews, *Phys. Rev. C* **108**, L031304 (2023).
- [36] W. I. Jay and E. T. Neil, *Phys. Rev. D* **103**, 114502 (2021).
- [37] See Supplemental Material at <http://link.aps.org/supplemental/10.1103/PhysRevC.109.035502> for the differential muon capture rate on deuterium.
- [38] R. J. Furnstahl, N. Klco, D. R. Phillips, and S. Wesolowski, *Phys. Rev. C* **92**, 024005 (2015).
- [39] A. S. Meyer, A. Walker-Loud, and C. Wilkinson, *Annu. Rev. Nucl. Part. Sci.* **72**, 205 (2022).
- [40] J.-W. Chen, T. Inoue, X. Ji, and Y. Li, *Phys. Rev. C* **72**, 061001(R) (2005).
- [41] B. Acharya, L. E. Marcucci, and L. Platter, *J. Phys. G: Nucl. Part. Phys.* **50**, 095102 (2023).
- [42] A. Baroni, L. Girlanda, A. Kievsky, L. E. Marcucci, R. Schiavilla, and M. Viviani, *Phys. Rev. C* **94**, 024003 (2016).